Available online at www.sciencedirect.com
SCIENCE DIRECT®
PERGAMON
International Journal of Heat and Mass Transfer 46 (2003) 1341–1357
International Journal of HEAT and MASS TRANSFER
www.elsevier.com/locate/ijhmt

Structure of mixed convective longitudinal vortex air flow driven by a heated circular plate embedded in the bottom of a horizontal flat duct

J.L. Tuh, T.F. Lin *

Department of Mechanical Engineering, National Chiao Tung University, Hsinchu, Taiwan 30010, ROC

Received 29 January 2002; received in revised form 30 September 2002

Abstract

In this study experimental flow visualization combined with transient temperature measurement are conducted to investigate the structure of the buoyancy driven longitudinal vortex rolls in low Reynolds number mixed convective air flow through a horizontal flat duct with an isothermally heated circular disk embedded in the bottom plate of the duct for the Reynolds number ranging from 15.1 to 99.2 and Rayleigh number from 3506 to 29,493. How the circular geometry of the heated surface affects the longitudinal vortex flow characteristics is investigated in detail. The results indicate that the longitudinal vortex rolls (L-rolls) in the duct core are induced at more upstream locations than those near the duct sides, which is completely opposite to those induced in a duct with a uniformly heated bottom. Besides, the thermals driven by the circular heated surface are not evenly spaced in the spanwise direction and are slightly asymmetric. It is of interest to note that at a given Rayleigh number *Ra* the thermals are unstable at high Reynolds numbers, suggesting the existence of the inertia driven instability. Thus the L-rolls evolved from these thermals are also unstable with the presence of nonperiodic generation and disappearance of new L-rolls. But at slightly lower *Re* the thermals and L-rolls are steady and regular. The vortex flow becomes unstable and irregular for a further reduction in the Reynolds number, which obviously results from the buoyancy driven instability. The simultaneous presence of these two instability mechanisms explains the appearance of the reverse steady–unsteady transition in the vortex flow.

Based on the present data, a flow regime map is given to delineate various L-roll patterns driven by the circular heated plate. In addition, the boundaries separating these patterns are empirically correlated. Empirical correlations for the onset points of the L-rolls are also provided.

1. Introduction

Buoyancy driven vortex flow and the associated thermal characteristics in mixed convection of gas moving through a bottom heated horizontal flat duct have been the subject of many investigations in recent years because of the important role they play in the growth of thin semiconductor crystal films from the metal-organic chemical vapor deposition (MOCVD) processes. A number of vortex flow patterns were identified and they were examined in some detail. In these investigations, the rectangular bottom and top plates of the duct are respectively heated and cooled uniformly. However, in the practical MOCVD processes the vapor flow is significantly affected by the buoyancy generated by the heated circular substrate as it moves over the substrate. The buoyancy induced flow is known to be very sensitive to the geometry of the heating surface [1]. Thus the vortex flow driven by the circular heated surface is expected to be somewhat different from that by the rectangular surface. Up to the present the mixed convective vortex flow over a circular plate is still rarely studied and hence poorly understood. In the initial

* Corresponding author. Tel.: +886-35712121/55118; fax: +886-35726440.
E-mail address: t7217@cc.nctu.edu.tw (T.F. Lin).

0017-9310/03/$ - see front matter © 2002 Elsevier Science Ltd. All rights reserved.
PII: S0017-9310(02)00425-8

Nomenclature

A	aspect ratio, b/d
b, d, l	test section width, height, length
g	gravitational acceleration
Gr	Grashof number, $\beta g d^3 \Delta T/\nu^2$
Ra	Rayleigh number, $\beta g d^3 \Delta T/\alpha\nu$
Ra_c	critical Rayleigh number corresponding to onset of convection
Re	Reynolds number, $W_m d/\nu$
Gr/Re^2	buoyancy-to-inertia ratio
t	dimensional time, s
T	temperature
T_{in}, T_{cp}	temperature at inlet of the test section and the circular copper plate
ΔT	$T_{cp} - T_{in}$
W	velocity components in axial direction
W_m, W_{max}	mean and maximum speeds of air in axial direction
x, y, z	dimensionless Cartesian coordinates scaled with b, d, l
θ	dimensionless temperature, $(T - T_{in})/\Delta T$
θ_{ave}	time averaged dimensionless temperature, $(T_{ave} - T_{in})/\Delta T$
α	thermal diffusivity
β	thermal expansion coefficient
ν	kinematic viscosity

attempt of the present study, combined flow visualization and temperature measurement will be conducted here to explore various aspects of the longitudinal vortex flow of air generated by a circular heated surface in a low Reynolds number mixed convective flow through a horizontal flat duct.

In the following, the relevant literature on the present study of mixed convective vortex flow of gas in a bottom heated horizontal flat duct is briefly reviewed. It has been known for some time that the onset of the secondary flow due to thermal instability is independent of the Reynolds number of the imposed main flow and always occurs at the critical Rayleigh number Ra_c of 1708 in a horizontal plane channel heated uniformly from below [2,3]. Beyond this critical Rayleigh number, steady longitudinal vortex rolls with spanwise symmetry prevail and the roll diameter is nearly equal to the duct height. The associated spanwise temperature distribution is in regular sinusoidal shape and the total number of the vortex rolls is equal to the aspect ratio of the duct. Ostrach and Kamotani [3,4] experimentally noted that the regular sinusoidal temperature distribution became distorted for $Re = 38$ as $Ra > 8000$. In a mixed convective air flow through a horizontal flat duct, Chang et al. [5] further revealed that the longitudinal vortices first came into view near the vertical sidewalls and then propagated to the interior of the duct. They also noted that the vortex flow became unsteady and asymmetric due to the presence of roll splitting and merging at high Rayleigh numbers. Rosenberger and his colleagues [6,7] observed unsteady snaking longitudinal vortex rolls even for the slightly supercritical Rayleigh number in mixed convection of nitrogen gas. Besides, the asymmetric roll patterns were also noted at low Rayleigh numbers. Moreover, they reported the data for the average axial distances measuring from the duct inlet for the onset of longitudinal rolls and for the rolls to become fully developed. Moffat and Jensen [8,9] numerically showed that the longitudinal vortex flow was very sensitive to the thermal boundary condition, duct aspect ratio and the carrier gas in the duct. Kamotani et al. [10] experimentally revealed the mushroom-shape flow structures near the onset point and indicated that the Nussult number on the heated plate depended mainly on the Rayleigh number but to a certain degree also influenced by the buoyancy-to-inertia ratio Gr/Re^2 especially when the ratio was much larger than unity.

Numerical simulation of the steady mixed convective longitudinal vortex flow in the horizontal flat duct was carried out by Ou et al. [11], Chou and Hwang [12] and Mahaney et al. [13]. They neglected the axial viscous and thermal diffusion in the simulation. Thus, the flow is parabolic and can be solved efficiently by various marching techniques. In view of the possible presence of the three-dimensional transient transional flow in the duct, this approximation becomes inappropriate at high Rayleigh numbers. To explore the buoyancy induced flow transition in the mixed convective air flow in a horizontal plane channel, recently Huang and Lin [14,15] directly solved the unsteady three-dimensional elliptic flow equations. They showed the formation, merging and splitting of the longitudinal rolls for the laminar steady, laminar time periodic, transitional quasiperiodic and irregular chaotic flow at increasing buoyancy-to-inertia ratio. The flow visualization from Osbrone and Incropera [16,17] distinctly disclosed four flow regimes along the bottom plate—laminar forced convection, laminar mixed convection, transitional mixed convection and turbulent free convection. The transition to turbulent flow was attributed to the breakdown of the vortices due to the hydrodynamic instability [18]. A similar study from Cheng and Shi [19] observed the convective instability of the air flow in the thermal entrance region of a horizontal rectangular channel. Their

results clearly revealed the complex secondary flow patterns caused by the buoyancy and the transition from laminar to turbulent flow.

The above literature review clearly indicates that to the best knowledge of the authors no study has been carried out to explore the detailed characteristics of the mixed convective vortex flow driven by the heated circular plate in a horizontal flat duct. In the present study an experiment combining flow visualization and temperature measurement will be conducted to explore the buoyancy driven mixed convective vortex flow of air over a heated isothermal circular plate embedded in the bottom plate of a horizontal flat duct. Comprehensive instantaneous temperature measurement will provide the data to delineate the unstable flow oscillation in the duct. Attention will be mainly focused on the longitudinal vortex flow. Effects of the Reynolds and Rayleigh numbers on the flow and thermal characteristics will be examined in detail.

2. Experimental apparatus and procedures

An open-loop mixed convection apparatus with air flowing through a horizontal high aspect ratio rectangular duct, which acts as the test section for the flat duct, is established in the present study to model the buoyancy driven vortex flow in a horizontal MOCVD reactor. The major constituents of the apparatus and the associated experimental procedures are briefly described in the following.

2.1. Experimental apparatus

A sketch of the experimental apparatus for the mixed convective air flow over a heated circular plate in a horizontal plane channel and the adopted coordinate system are schematically shown in Fig. 1. The apparatus begins with the air regulated from a 300 l and 100 psi high-pressure tank. Then, the air passes through a settling chamber, a contraction nozzle and a developing channel before entering the test section. After leaving the test section, the air is sent through the exhaust portion and is discharged into the ambient.

The test section has a cross-section of 22.5 mm in height and 450 mm in width, providing an aspect ratio A of 20, and has a total length of 450 mm. The side and top walls of the duct are constructed of 10-mm thick transparent acrylic plates to allow for the visualization of vortex flow patterns. The bottom of the test section is a thick flat bakelite plate embedded with a 15-mm thick, high purity circular copper plate of 300 mm in diameter to model a 12-in. semiconductor wafer. The upper surfaces of the bakelite and copper plates are kept at the same horizontal level so that the air flow does not experience any step when moving over the copper plate. To obtain the uniform plate temperature, the heating elements attached onto the lower surface of the copper plate are divided concentrically into seven zones and the heater for each zone is independently controlled by a GW GPC 3030D laboratory power supply. Besides, a mica sheet is placed between the copper plate and heating elements to prevent the electric current leaking to the copper plate (Fig. 2). With a suitable control of the power supplies the copper plate can be maintained at a nearly uniform temperature.

A good control of the flow condition upstream of the test section is also essential and is considered in the design of the experiment. More specifically, at the inlet of the loop the working fluid (air) is driven by a 7.5 hp air compressor and sent through a dryer installed with water vapor and oil filters. The dry air then moves into the high-pressure tank. To proceed with the experiment, the air flow is further controlled by a pressure regulator and its volume flow rate is measured by a Brooks 5851E flow controller with an accuracy of 1%. Through a flexible tube, the air enters the settling chamber, in which four fine-mesh screens, a divergent buffer section, a honeycomb and another four fine-mesh screens are installed in sequence to reduce the turbulence in the air flow. The air turbulence is further suppressed by passing the air through a contraction nozzle with a contraction ratio of 44:1, which provides a nearly uniform flow at the inlet of the developing section.

The developing section is 1400-mm in length, $\approx$62 times of the duct height. This insures the flow to be fully developed at the inlet of the test section for $Re \leqq 100$. An insulated outlet section of 450-mm long is added to the test section to reduce the effects of the disturbances from discharging the flow to the ambient. The developing and outlet sections are both made of 10-mm thick acrylic plate, whereas the settling chamber and contraction nozzle are made of stainless steel plates. The settling chamber and the developing, test and outlet sections are all thermally insulated with a 20-mm thick Superlon insulator and the entire loop is fixed on a rigid supporting frame.

Visualization of the buoyancy driven vortex flow in the test section is realized by injecting smoke at some distance ahead of the settling chamber. The smoke is produced by a smoke generator, which is a cubic space with the incense burned in it. Note that the particles from the incense burning are fine enough so that they can move with the vortex flow. By keeping the smoke concentration at a suitable level, the incense particles can be illuminated by a plane light sheet from a 550 W overhead projector. With an adjustable knife edge a sharp contrast could be achieved between the duct walls and smoke. The flow photos from the top, side and end views of the test section can then be taken. The exposure time is about 1/125 s in taking the photos.

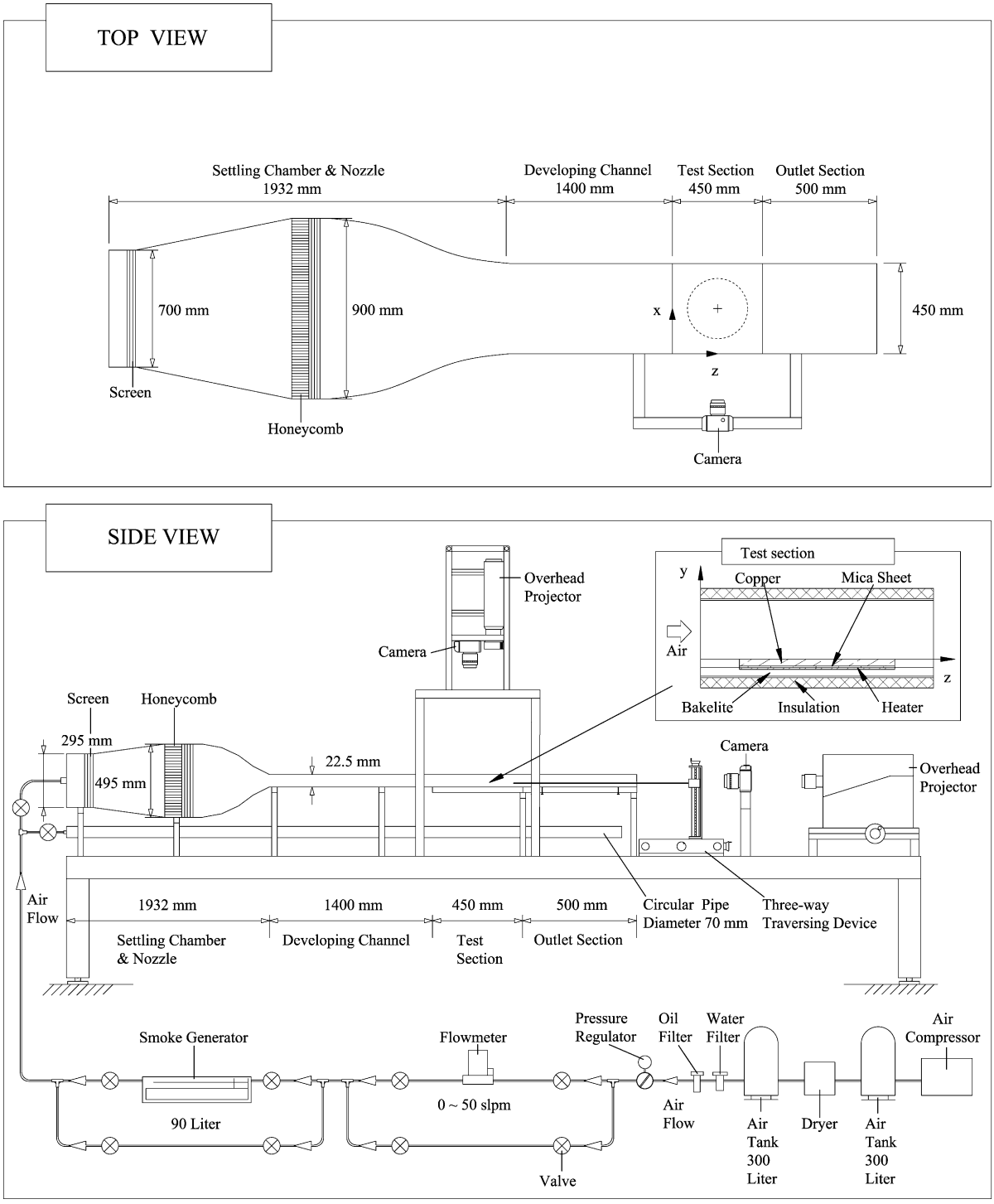

Fig. 1. Schematic of experimental apparatus and the chosen coordinate system for the test section.

The temperature of the heated copper plate is measured by 17 calibrated and electrically insulated T-type thermocouples embedded at selected locations in the plate. The thermocouple beads are fixed at about 1 mm from the upper surface of the copper plate through the small holes drilled from the back side of the plate.

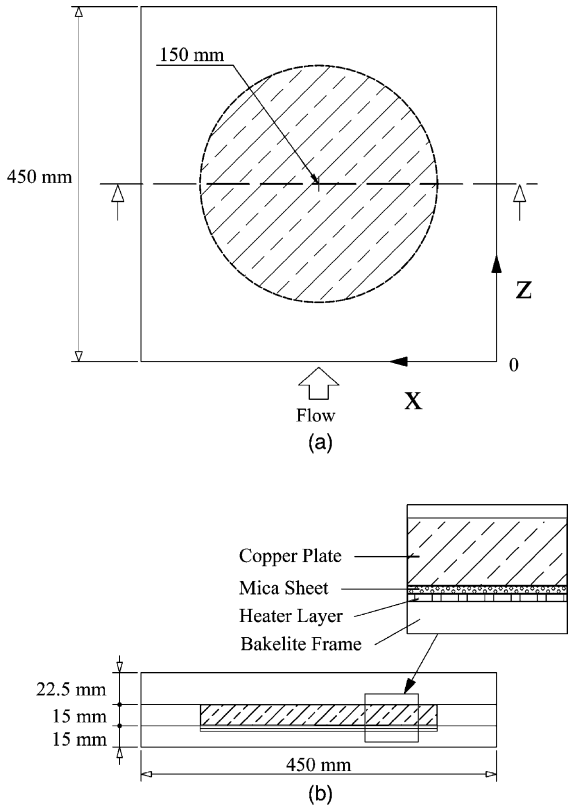

Fig. 2. Schematic of the test section from (a) top view and (b) cross-sectional view showing the design of the bottom plate.

A calibrated T-type thermocouple is also used to measure the inlet air temperature at locations just upstream of the test section. The signals from the thermocouples are recorded by the Hewlett-Packard 3852A data acquisition system with a resolution of ±0.05 °C.

To measure the temperature distribution of the air flow in the flat duct, a calibrated thermocouple probe is inserted from the downstream end of the test section. The probe is supported by a three-way traversing device. More specifically, the thermocouple probe is an OMEGA (model HYP-O) mini hypodermic extremely small T-type thermocouple (33 gauge) implanted in a 1 in. long stainless steel hypodermic needle. This movable thermocouple probe can measure the time-average and instantaneous temperature of the flow. The temperature data are recorded when the flow reaches steady or statistically stable state, usually 5–6 h after starting the test. It was noted that in all tests the maximum temperature differences between any two locations in the copper plate were below 0.1 °C. The error in the temperature difference between the copper surface and the air at the duct inlet is estimated to be within ±0.1 °C.

2.2. Analysis of time-average and instantaneous air temperature

The time-average temperature distributions in the air flow are obtained by averaging 1000–3000 sampled data at each detection point. The period of the sampling time may be different for different cases. Most importantly, the period has to be long enough to capture all the slowest temperature oscillations in the air flow. The response time of the thermocouple is about 0.12 s and the sampling rate was about 5 Hz in the transient temperature measurement. This sampling rate is high enough for the present low Reynolds number mixed convection experiment.

2.3. Preliminary investigations of flow field

In order to confirm the fully developed condition at the entrance of the test section, measurements using a hot-wire anemometer (DANTEC probe Type 55P01 with 56C17 CTA bridge) in connection with a HP data acquisition system (the Hewlett-Packard VXI series-E1411B multimeter and E-1347A multiplexers) for the inlet velocity profiles are conducted. For calibrating the hot wire, the pipe-flow method that the probe is placed in the center of a fully developed laminar pipe flow is used. The total volume flow rate is estimated and the pipe center velocity is calculated from the parabolic distribution. Fig. 3 shows the measured velocity profiles along the vertical centerline at $x = 0.5$ and horizontal centerline at $y = 0.5$ for $Re = 100$ with no heat input to the circular copper plate. The measured data are in good agreement with the analytical results given by Shah and London [20]. The turbulence level of the inlet stream is also given in the figure and is all within 1%. This implies that the effects of the free stream turbulence on the mixed convective flow characteristics are moderate.

2.4. Experimental procedures

For convenience, experiments are designated according to the Reynolds and Rayleigh numbers based on the inlet conditions and the mean air speed in the test section calculated from the total flow rate. In each test the flow controller is first set at the predetermined level to impose a desired, fully developed flow through the entire test section. The power supplies are then turned on to raise the copper plate temperature. Usually, it takes about 3 h for the Rayleigh number to be raised to the test point and another 2 h are needed to maintain the vortex flow at steady or statistically stable state. The steady state is ascertained by insuring that the variation in the instantaneous temperature measured in the flow from each thermocouple be less than ±0.1 °C for a period of at least 25 min. The above choice of the steady state criterion is in accordance with the fact that the measured

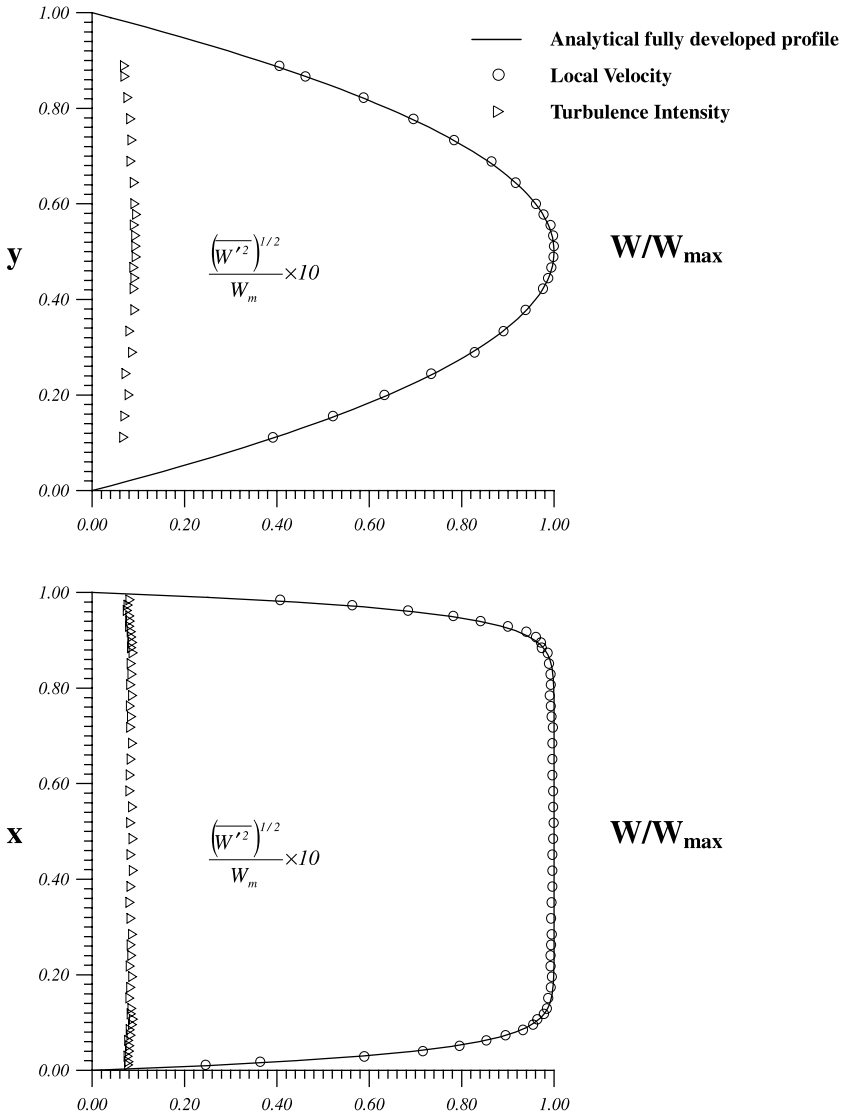

Fig. 3. Comparison of the measured axial velocity profiles $W/W_{\max}$ at the inlet of test section with the analytical solution from [20] for $Re = 100$ at (a) $x = 0.5$ and (b) $y = 0.5$.

background temperature disturbances in the flow are found to be slightly less than ±0.1 °C. On the other hand, the statistically stable state is considered to be reached when the variation of the time-average temperature in the flow is within ±0.1 °C for more than 25 min. After the steady or statistically stable state is reached, we start the temperature measurement and flow visualization.

2.5. Uncertainty analysis

Uncertainties in the Rayleigh number *Ra*, Reynolds number *Re* and other independent parameters are estimated in the light of the standard procedures proposed by Kline and McClintock [21]. The uncertainties of the thermophysical properties of air are included in the analysis. The fundamental thermophysical properties of the working fluid (air) are $\alpha = 0.22$ (cm^2/s), $\beta = 0.0034$ (1/K) and $\nu = 0.162$ (cm^2/s) at 30 °C and 0.997 bar. The fluid properties are further corrected based on the temperature and pressure detected at the inlet of the test section. In addition, the deviation of the temperature among the detecting points in the circular copper plate and the control unsteadiness are also accounted for in the evaluation of the data uncertainties. The analysis shows that the uncertainties of temperature, volume flow rate, dimensions, Reynolds number and Rayleigh number measurements are estimated to be less than ±0.15 °C, ±1%, ±0.05 mm, ±3% and ±5%, respectively.

3. Results and discussion

Selected results from the present study will be presented in the following to illustrate the characteristics of the longitudinal vortex rolls induced in a low Reynolds number mixed convective air flow over a circular heated plate. How the particular geometry of this circular heated plate affects the vortex flow characteristics will be examined in detail. In the experiment the Reynolds number of the flow is varied from 15.1 to 99.2 and Rayleigh number from 3506 to 29,493 covering the steady and time-dependent longitudinal vortex flows. The ranges of *Re* and *Ra* covered here are in accordance with the actual chemical vapor deposition processes [22].

3.1. Onset of longitudinal rolls

To manifest the onset of the longitudinal rolls (L-rolls) induced by the heated circular plate, a typical steady regular longitudinal vortex flow is shown in Fig. 4 by presenting the steady top and end view flow photos respectively taken at the middle horizontal plane $y = 0.5$ and at selected cross-sections for the case with $Re = 24.8$ and $Ra = 9215$. In Fig. 4(b)–(j) and some other figures to

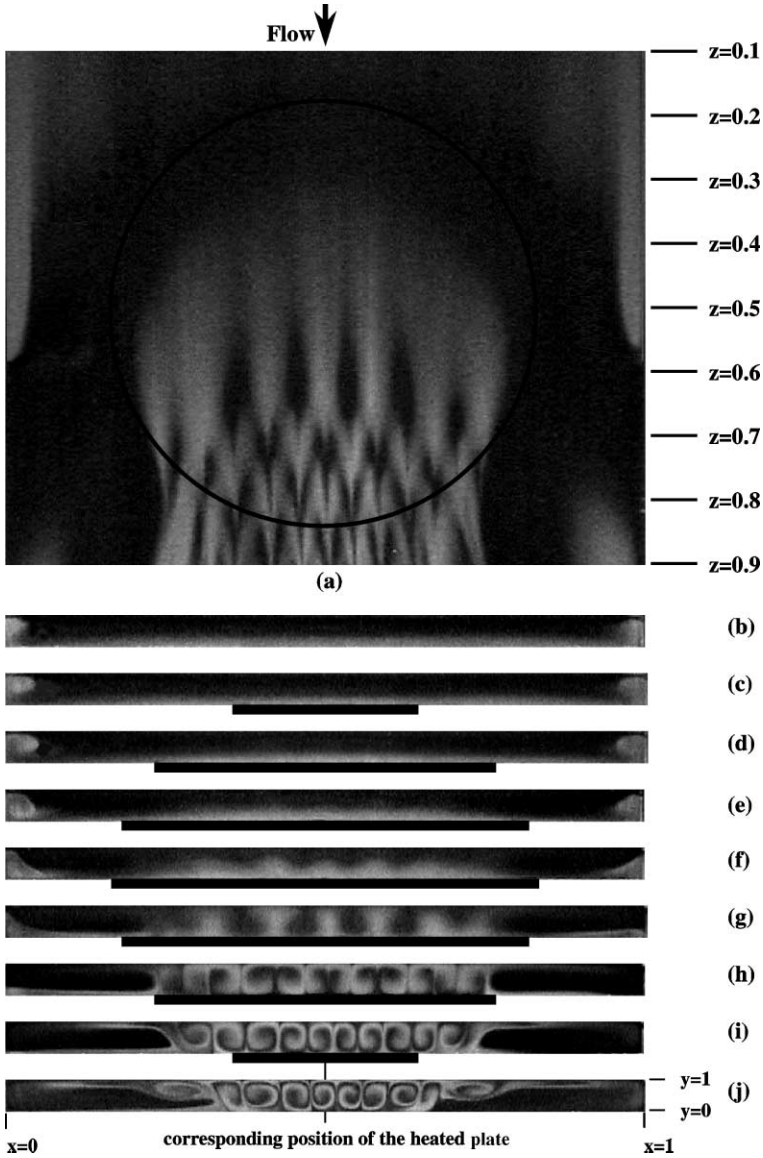

Fig. 4. Top view flow photo taken at $y = 0.5$ (a) and end view flow photos taken from the planes: $z =$ (b) 0.1, (c) 0.2, (d) 0.3, (e) 0.4, (f) 0.5, (g) 0.6, (h) 0.7, (i) 0.8 and (j) 0.9 at steady state for $Re = 24.8$ and $Ra = 9215$.

be examined later the thick black underlines below the end view flow photos signify the presence of the heated circular plate. The results clearly show the appearance of the L-rolls right above the exit half of the circular plate. We also note that an axially slender, weakly recirculating flow zone exists near each sidewall of the duct and extends from the entry half of the test section to the far upstream region beyond the test section inlet. These two flow recirculations are essentially the reverse flow resulting from the retardation of the main forced flow by the vertically upward buoyancy associated with the heated circular plate. A close inspection of the longitudinal vortex flow above the plate reveals that prior to the formation of L-rolls (Fig. 4(h)) several thermals rise from the heated plate (Fig. 4(f) and (g)). Under the simultaneous action of the forced flow and buoyancy, these thermals grow slowly in the upward and downstream directions and become elongated with mushroom-like cross-sections. A continuing growth of the thermals causes them to evolve into L-rolls after the thermals hit the duct top. Note that because of the circular geometry of the heated plate, closer to the duct core the thermals are induced at more upstream locations. This is very different from the onset of L-rolls over a heated rectangular plate in which the rolls first appear in the sidewall region and the rolls in the duct core are initiated at somewhat downstream locations [5]. To quantify the onset locations, we need to choose a suitable and practical criterion for the onset of L-rolls. Here the roll onset is considered to occur at the particular location where a thermal just rises to the midheight of the duct. Hence the onset point can be directly read from the top view flow photos which are taken at the midheight of the duct. Based on the present data, the onset locations of the steady regular L-rolls can be correlated as

$$z_{\text{onset}}^2 = z_{\text{c,onset}}^2 + 2\left(x - \frac{1}{2}\right)^2 \tag{1}$$

where $z_{\text{c,onset}}$ is the onset location for the two L-rolls in the duct core around the central vertical plane $x = 0.5$ and it can be expressed empirically as

$$z_{\text{c,onset}} = 1/6 + 20\left(\frac{Re^{1.2}}{Ra}\right)^{0.8} \tag{2}$$

The above equations can predict our data with an average deviation less than 12%.

3.2. Characteristics of longitudinal rolls

Some prominent characteristics of the steady L-rolls unique to the vortex flow driven by the circular heated plate are noted from the typical flow photos presented in Fig. 4. More specifically, all the L-rolls do not have the same size. Instead, the L-rolls near the central vertical plane $x = 0.5$ are the smallest and they become somewhat wider in the region closer to the sidewall of the test section, as evident from the end view flow photo for $z = 0.8$ (Fig. 4(i)). Besides, the rolls appear in the region closer to the central vertical plane are stronger. It is of interest to note that the vortex structure of the L-rolls can persist to some distance well into the region downstream of the circular plate (Fig. 4(j)) except in the region near the duct sides where the decay of the L-rolls is substantial. Furthermore, the L-rolls are not completely spanwisely symmetric. Some vortex flow asymmetry can be discerned. Additionally, the rolls do not become fully developed in the duct. The above characteristics of the L-rolls are also seen in the corresponding spanwise distributions of the dimensionless time-average air temperature measured at the midheight of the duct shown in Fig. 5. It should be pointed out from the results in Fig. 5 that the decay of the sinusoidal temperature variation

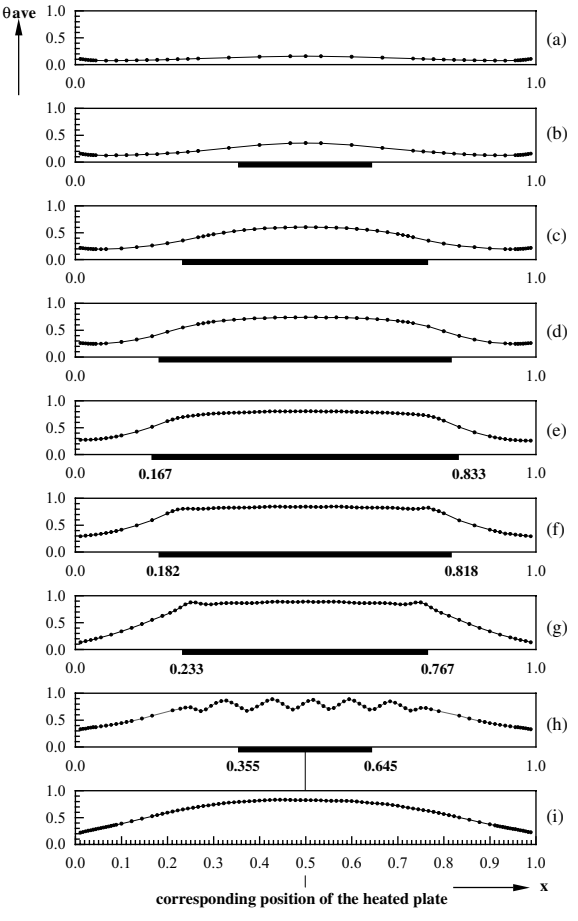

Fig. 5. Spanwise time-average air temperature distributions on the plane $y = 0.5$ and at selected cross-sections $z =$ (a) 0.1, (b) 0.2, (c) 0.3, (d) 0.4, (e) 0.5, (f) 0.6, (g) 0.7, (h) 0.8 and (i) 0.9 for $Re = 24.8$ and $Ra = 9215$.

driven by the longitudinal rolls is relatively quick as the flow leaves the circular plate, unlike the vortex flow structure.

Next, the longitudinal vortex flow structures at increasing buoyancy-to-inertia ratio by lowering the Reynolds number at a low buoyancy are illustrated in Fig. 6 by showing the top view flow photos at various Re for Ra around 10,536 at steady or statistically stable state. The results indicate that at the low buoyancy-to-inertia ratios with $Re = 82.3$ and 61.5 only some thermals are induced in the exit half of the test section (Fig. 6(a) and (b)). Note that at this low Gr/Re^2 the buoyancy driven thermals do not possess enough momentum to rise to the top plate of the duct to form L-rolls. Apparently, it takes a shorter distance for the thermals to be initiated for a higher Gr/Re^2. We further note that only in the duct core the thermals are evenly spaced in the spanwise direction. The thermals induced in the region near the side edge of the circular plate are much weaker. They are slightly unstable and irregular to

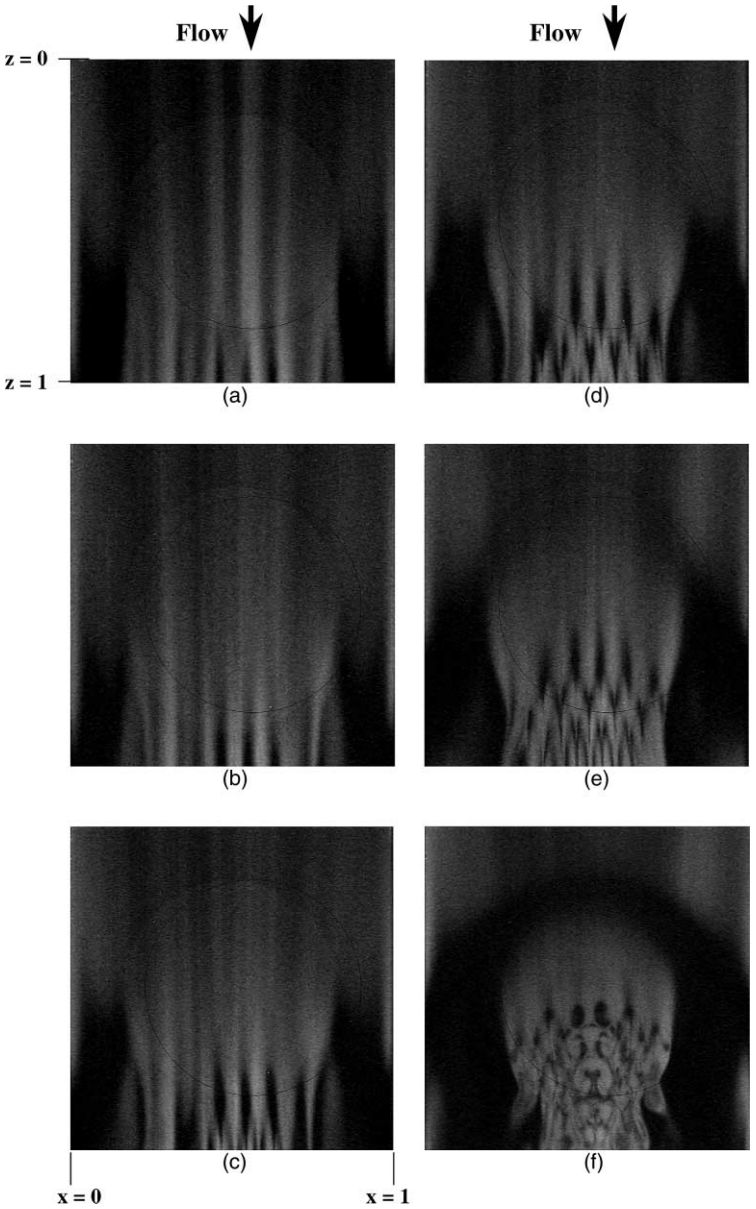

Fig. 6. Top view flow photos at steady or statistical state for $Ra = 10{,}536$ on the plane $y = 0.5$ for $Re =$ (a) 82.3, (b) 61.5, (c) 51.2, (d) 40.7, (e) 30.4 and (f) 15.1.

a certain degree. As the Reynolds number is lowered to 51.2 the thermals in the duct core evolve to L-rolls near the test section exit (Fig. 6(c)). For a further reduction of *Re* to 40.7 and 30.4 all the thermals eventually evolve to L-rolls (Fig. 6(d) and (e)). Obviously, the onset points of the L-rolls move upstream for a lower *Re*. At an even lower *Re* of 15.1 the buoyancy-to-inertia ratio is very high and the vortex flow in the duct becomes somewhat irregular (Fig. 6(f)). In fact, this irregular vortex flow is time dependent and will be examined later. It is worth mentioning that even at low Gr/Re^2 the L-rolls away from the duct core, which evolve from the slightly irregular thermals in the upstream, are somewhat irregular (Fig. 6(c) and (d)).

To further illustrate the effects of the Reynolds number on the longitudinal vortex flow, the top view flow photos at the steady or statistically stable state for the higher Rayleigh number of 18,610 at various *Re* are presented in Fig. 7. These results when contrasted with those in Fig. 6 for $Ra = 10{,}536$ reveal that at the higher *Ra* the thermals driven at the higher *Re* ($\geqslant 70$) are more unevenly spaced (Fig. 7(a)–(c)). Besides, the spanwise asymmetry in the patterns of the L-rolls is more severe and the vortex flow does not have steady state for

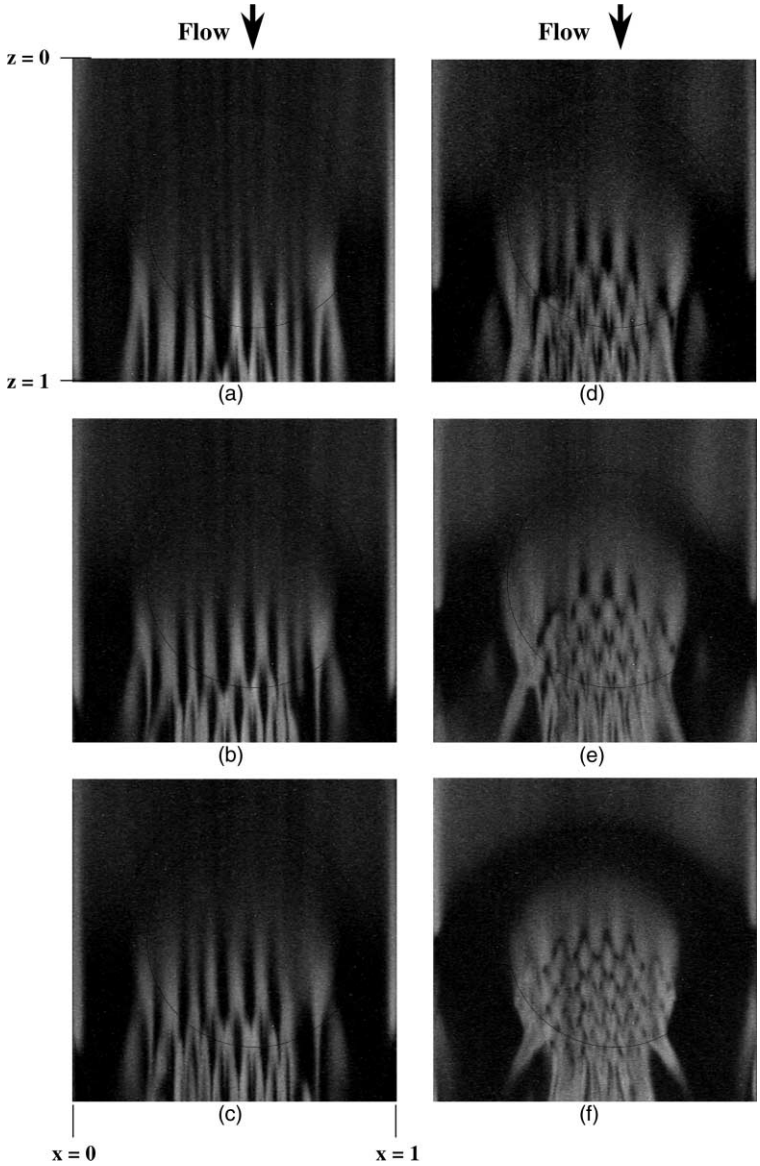

Fig. 7. Top view flow photos at steady or statistical state for $Ra = 18{,}610$ on the plane $y = 0.5$ for *Re* = (a) 99.2, (b) 82.3, (c) 71.8, (d) 51.2, (e) 40.7 and (f) 24.8.

$Re \geqslant 50$. For some cases, generation and disappearance of the L-rolls take place in the region near the downstream edge of the circular plate (Fig. 7(c)). The generation and disappearance of the rolls can be clearly seen by the end view flow photos shown in Fig. 8 for $z = 0.9$ at selected time instants at the statistical state. In Fig. 8 the time $t = 0$ denotes a certain arbitrary time instant at the statistical state and the arrowheads are used to point out the region in which the roll generation and disappearance take place. Note that in the right half of the test section the rolls show little change with time and are relatively stable. But in the left half of the test section and in the region near the edge of the circular plate we note that a new thermal begins to rise from the duct bottom at $t = 0$ (Fig. 8(a)). Then, the thermal grows quickly and squeezes the rolls in the neighborhood (Fig. 8(b) and (c)). At $t = 6.3$ s a big L-roll forms (Fig. 8(d)). As time continues to increase, this newly formed roll gradually decays (Fig. 8(e) and (f)). The roll is rather weak at $t = 14.6$ s (Fig. 8(g)). Finally at $t = 20.5$ s the roll completely disappears (Fig. 8(h)). These generation and disappearance of the L-rolls are found to occur cyclically in the flow but in a time nonperiodic manner.

It is of interest to further note from the flow visualization for the cases shown in Fig. 7 that as Re is lowered from 71.8 to 51.2 and 40.7 for Ra fixed at 18,610 the resulting vortex flow is steady and is almost spanwisely symmetric (Fig. 7(d) and (e)). More detailed vortex flow structure for $Re = 40.7$ and $Ra = 18{,}610$ at steady state is shown in Fig. 9 and the corresponding spanwise distributions of the dimensionless time-average air temperature measured at the middle horizontal plane of the test section are shown in Fig. 10. Thus, we have a rather unusual phenomenon of the flow transition from unsteady to steady states at increasing buoyancy-to-inertia ratio, which is known as the reverse flow transition. This is considered to be the consequence that the buoyancy induced thermals from a heated circular plate are more unstable in the flow of higher Reynolds number. For a further lowering of Re to 24.8 the L-rolls become unstable (Fig. 7(f)). This flow transition from steady to unsteady states at increasing Gr/Re^2 is normally seen in most mixed convective flow systems [14]. In summary, there are two flow transitions between the steady and unsteady states at increasing buoyancy-to-inertia ratio for a high Rayleigh number in the longitudinal vortex flow driven by the heated circular surface.

Then, the effects of the Rayleigh number on the longitudinal vortex flow pattern are demonstrated in Fig. 11 by showing the results for $Re = 40.7$ and Ra varying from 3506 to 29,493 at steady or statistically stable state. The results clearly indicate that even for

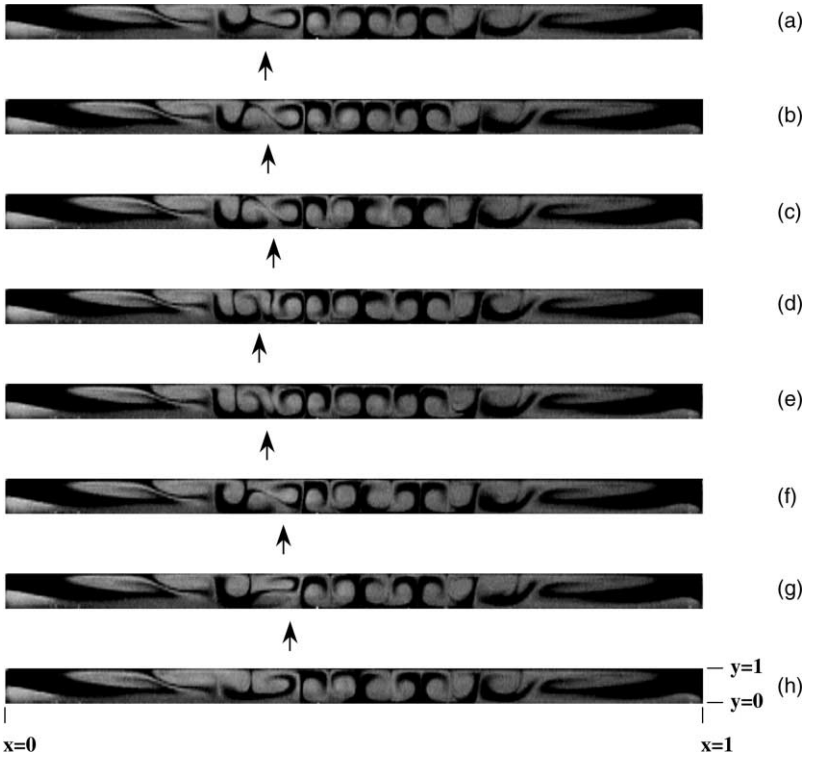

Fig. 8. Cross-sectional view flow photos showing the new generation of a thermal at $z = 0.9$ for $Re = 71.8$, $Ra = 18{,}610$ and $t =$ (a) 0 s, (b) 1.0 s, (c) 5.1 s, (d) 6.3 s, (e) 9.1 s, (f) 11.5 s, (g) 14.6 s, and (h) 20.5 s.

$Ra = 3506$, which is well above the critical Rayleigh number for the onset of L-rolls ($Ra_c = 1708$) in a long horizontal plane channel heated uniformly from below, no thermals and rolls are detected (Fig. 11(a)). The flow is still uni-directional and forced convection dominated. The much higher critical Rayleigh number needed in the present study to induce the vortex flow is attributed to the finite size of the heated circular plate considered here. At the higher *Ra* of 5880 thermals are seen in the test section (Fig. 11(b)). The thermals are almost spanwisely symmetric. As *Ra* is raised to 10,536 and 14,225, the thermals gradually develop into steady regular L-rolls, as evident from the steady top view flow photos given in Fig. 11(c) and (d). The vortex flow again is only slightly asymmetric. The upstream moving of the onset points of the L-rolls at increasing *Ra* is also clearly noted. For an even higher buoyancy with $Ra = 20{,}602$ and 29,493 (Fig. 11(e) and (f)), the longitudinal vortex flow becomes somewhat irregular and is time dependent especially in the region near the downstream edge of the circular plate. Besides, at these high *Ra* the spanwise symmetry of the L-rolls is broken to a certain

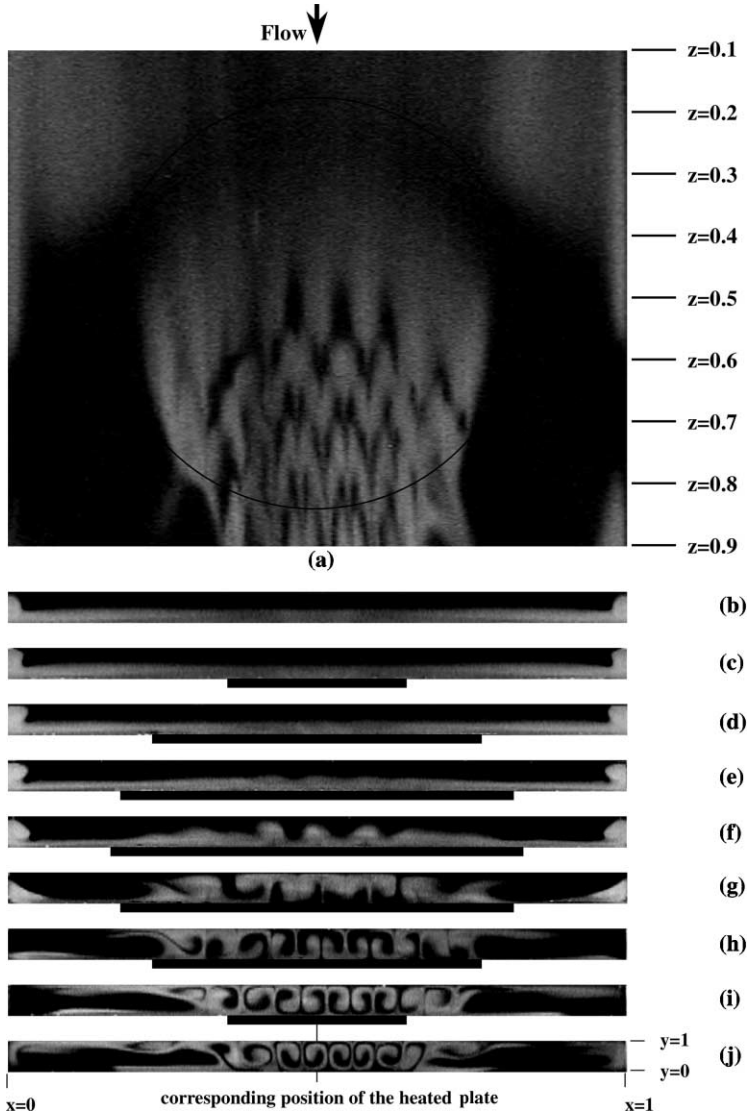

Fig. 9. Top view flow photo taken at $y = 0.5$ (a) and end view flow photos taken from the planes: $z =$ (b) 0.1, (c) 0.2, (d) 0.3, (e) 0.4, (f) 0.5, (g) 0.6, (h) 0.7, (i) 0.8 and (j) 0.9 at steady state for $Re = 40.7$ and $Ra = 18{,}610$.

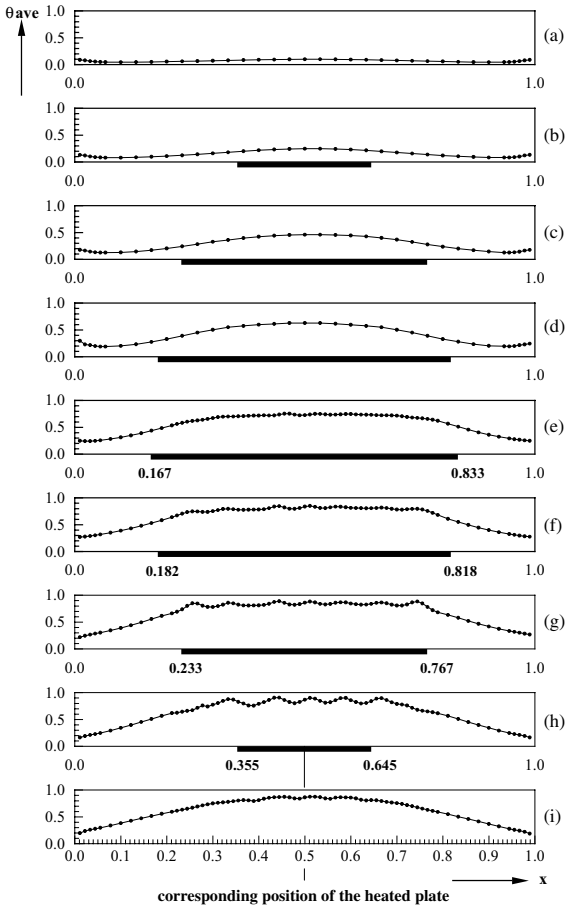

Fig. 10. Spanwise time-average air temperature distributions on the plane $y = 0.5$ and at selected cross-sections $z =$ (a) 0.1, (b) 0.2, (c) 0.3, (d) 0.4, (e) 0.5, (f) 0.6, (g) 0.7, (h) 0.8 and (i) 0.9 for $Re = 40.7$ and $Ra = 18{,}610$.

degree. The vortex flow near the exit of the test section is actually characterized by the highly distorted L-rolls which merge and split in a random order.

3.3. Transition to time dependent flow

In the above discussion we have mentioned that there exist two instability mechanisms for the mixed convective vortex flow considered here to become time dependent. One mechanism is associated with the instability of the buoyancy induced thermals caused by the increase of the Reynolds number of the main flow. This is considered as an inertia driven stability. Another mechanism results from the instability of the regular L-rolls due to the rising Rayleigh number. Obviously, this is a thermal instability. The simultaneous presence of these two instabilities results in a nonmonotonic trend in the flow transition to a time dependent state at increasing buoyancy-to-inertia ratio. It should be pointed out that the inertia driven instability of thermals is not noted in the duct heated uniformly from below [5].

Comprehensive instantaneous air temperature measurement combined with the flow visualization are performed here to delineate the boundaries between the steady and unsteady flow and to elucidate the temporal characteristics of the unsteady longitudinal vortex flow. The results from this measurement indicate that the longitudinal vortex flow becomes time dependent when

$$3.5 < Gr/Re^2 < 12 \quad \text{for} \quad 35 < Re < 100$$
$$\text{and} \quad Gr/Re^2 > 50 \quad \text{for} \quad 15 < Re < 35 \tag{3}$$

in the range of $8000 < Ra < 21{,}000$. Moreover, the data from the instantaneous temperature measurement suggest that the steady–unsteady transition in the present mixed convective longitudinal vortex flow is subcritical. This signifies that a steady flow abruptly changes to a nonperiodic time dependent flow for a very small variation in the Reynolds or Rayleigh number. No time periodic temperature oscillation is detected. Fig. 12 shows the time variations of the measured air temperature at selected locations at the midheight of the test section for a typical buoyancy driven unstable vortex flow with $Re = 15.1$ and $Ra = 10{,}536$. The results indicate that near the central vertical plane at $x = 0.5$ in the exit half of the test section the flow oscillates irregularly in a large amplitude. But outside this small region the flow is steady essentially, in view of the amplitude of the temperature oscillation being at the same order of the background disturbances.

3.4. Flow regime map

As discussed above, the vortex flow patterns observed in the present study include the thermals, regular L-rolls, inertia driven deformed L-rolls and buoyancy driven unstable deformed L-rolls. They are summarized in a flow regime map shown in Fig. 13. The results from this flow regime map clearly suggest that at a very low Gr/Re^2 the flow is still unidirectional and is forced convection dominated. For a higher buoyancy-to-inertia ratio by lowering the Reynolds number or increasing the Rayleigh number, thermals appear and eventually evolve to longitudinal vortex rolls at moderate Re when Ra is beyond 8000. It is of interest to note that the vortex flow driven by the circular heated plate is dominated by the thermals over wide ranges of Re and Ra. Besides, the induced vortex rolls lose their steadiness by the inertia driven instability at high Reynolds numbers and hence steady regular longitudinal vortex rolls exist only in a small region. For an even higher Gr/Re^2, the resulting longitudinal vortex flow becomes somewhat irregular.

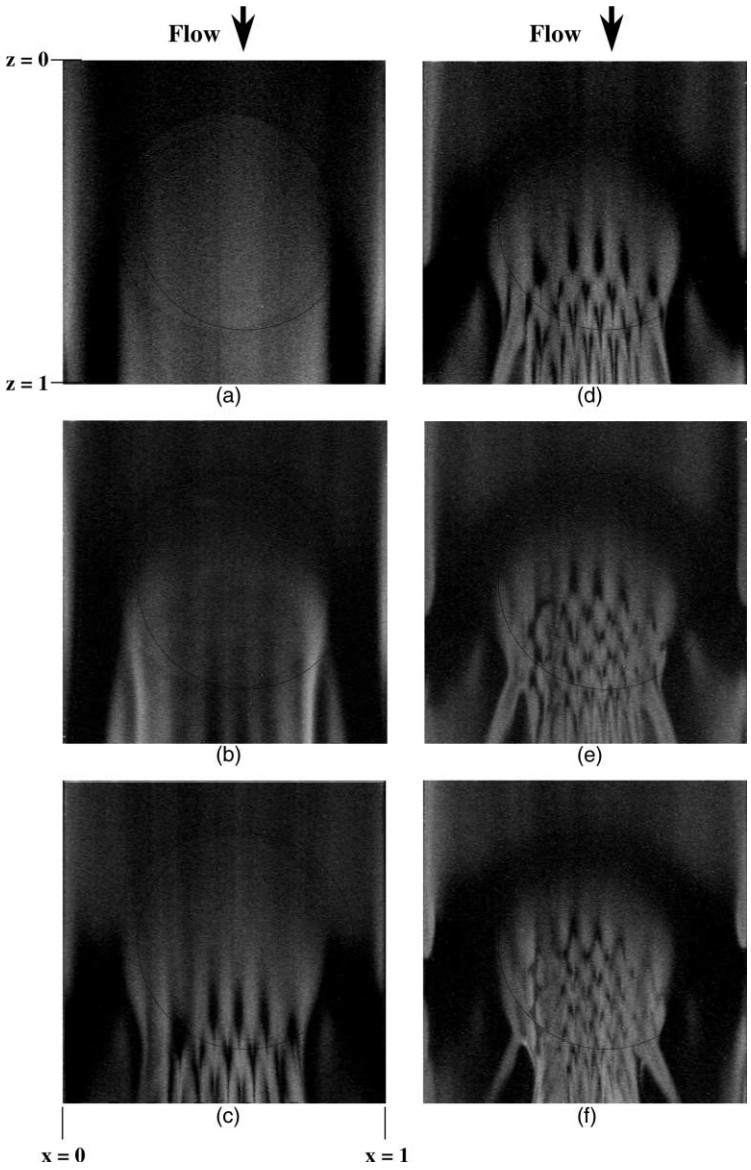

Fig. 11. Top view flow photos at steady or statistical state for $Re = 40.7$ on the plane $y = 0.5$ for (a) $Ra = 3506$, (b) $Ra = 5880$, (c) $Ra = 10{,}536$, (d) $Ra = 14{,}225$, (e) $Ra = 20{,}602$ and (f) $Ra = 29{,}493$.

Finally, the boundaries separating various vortex flow patterns in the present flow regime map can be empirically correlated as

$$Ra_{1\text{–}2} = 640 + 0.8Re^2 \tag{4}$$

$$Ra_{2\text{–}3} = 7200 + 1.6Re^2 \tag{5}$$

$$Re_{3\text{–}4} = -22 + 0.0076Ra - 2.1 \times 10^{-7}Ra^2 \tag{6}$$

$$Ra_{4\text{–}5} = 5400 + 27Re^2 \tag{7}$$

4. Concluding remark

An experiment combining flow visualization and temperature measurement has been carried out here to investigate the structure of the buoyancy driven longitudinal vortex rolls in mixed convective air flow through a horizontal flat duct with a circular heated plate embedded in the duct bottom for the Reynolds number ranging from 15.1 to 99.2 and Rayleigh number from 3506 to 29,493. The unique vortex flow characteristics driven by this particular geometry of the heated surface

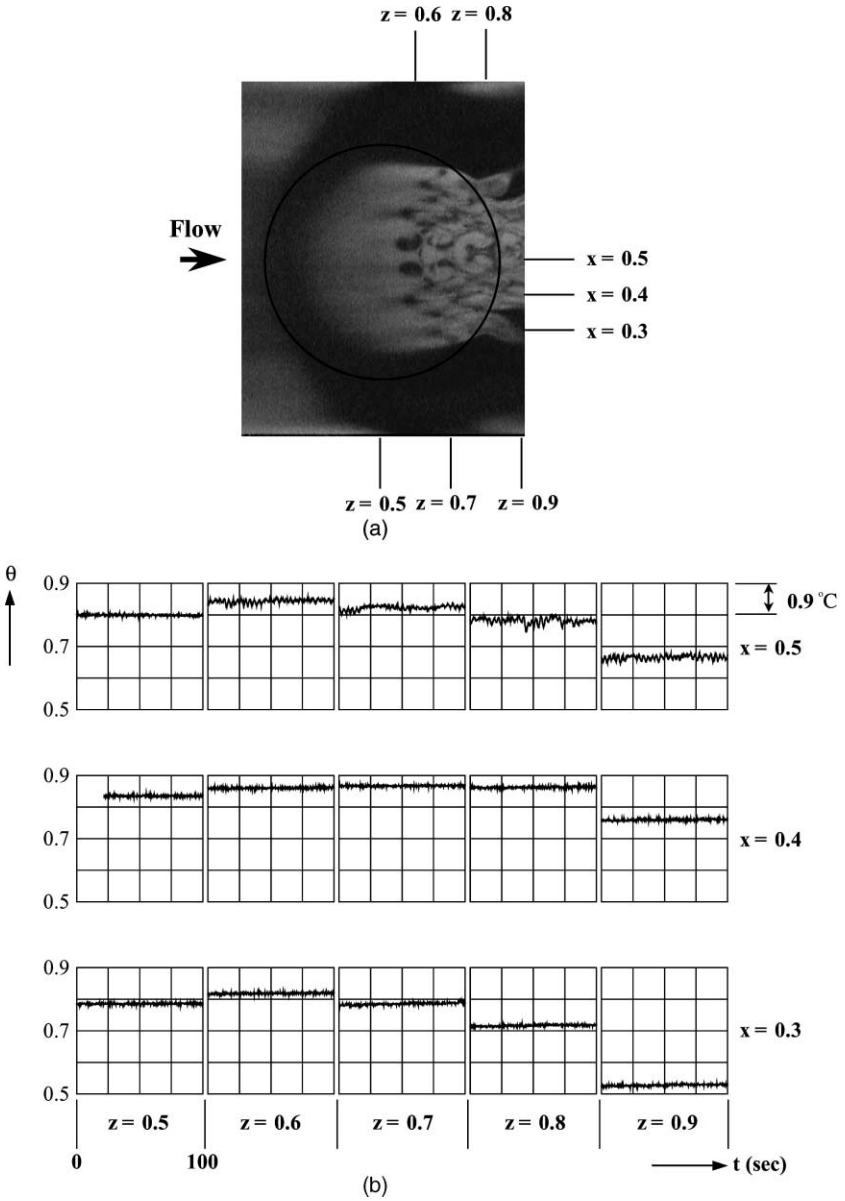

Fig. 12. Temporal structure of unsteady vortex flow from (a) top view photo and (b) time records of air temperature at selected locations on the plane $y = 0.5$ at $x = 0.5$, 0.4 and 0.3 for $Re = 15.1$ and $Ra = 10{,}536$.

were examined in detail. The major results obtained can be briefly summarized in the following.

(1) The circular geometry of the heated plate causes the L-rolls in the duct core to be induced at more upstream locations than those near the duct sides. This is completely different from that in a duct with a uniformly heated bottom.
(2) The thermals induced by the circular heated plate, which can later evolve to L-rolls, are not evenly spaced in the spanwise direction. At high Re ($\geqslant 50$) and Ra ($\geqslant 9200$) the thermals are unstable, and the L-rolls evolving from these unstable thermals are also unstable. Besides, nonperiodic generation and disappearance of new rolls can occur in the flow. But the L-rolls become steady and regular as Re is lowered to 40.7, 30.4 and 24.8. For a further reduction of Re to 20.2 and below the L-rolls become unstable and are somewhat irregular. Thus, we have a reverse flow transition in the duct.

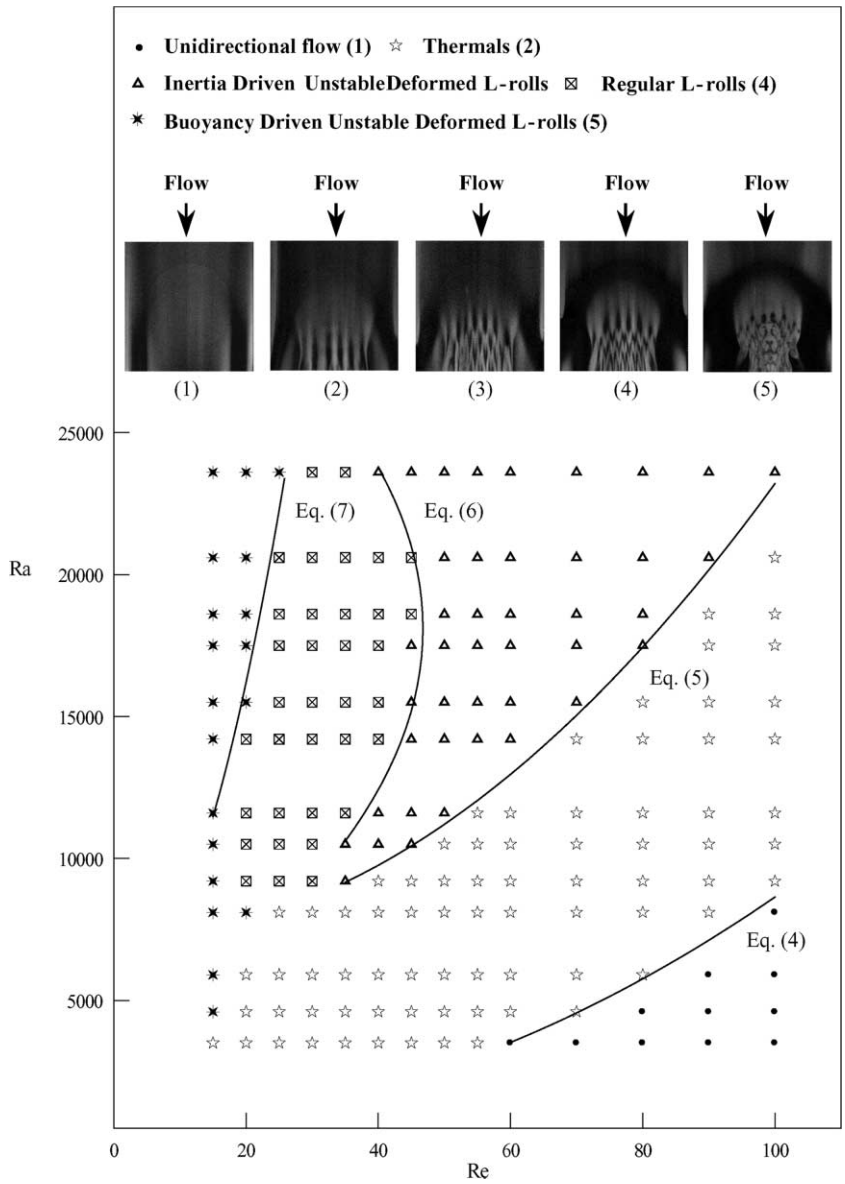

Fig. 13. Flow regime map for different flow patterns observed in flow visualization (182 cases).

(3) There are two types of instability in the vortex flow. The inertia driven instability results in the unstable thermals, which in turn results in the unstable L-rolls, at high *Re*. While at a high buoyancy-to-inertia ratio the buoyancy driven instability sets in, causing unstable L-rolls.
(4) The longitudinal vortex flow driven by the circular heated plate is prone to become slightly asymmetric and even the steady L-rolls do not have the same size.
(5) A flow regime map is provided to delineate various longitudinal vortex flow patterns in the duct. Besides, the boundaries separating these flow patterns are empirically correlated.

During the course of this study it has been realized that the vortex flow driven by the circular heated plate can be in the form of time periodic moving transverse rolls when the Reynolds number is lower than that considered in the present study. The detailed characteristics of the transverse rolls driven by the circular heated surface are expected to be somewhat different from those driven by the rectangular heated surface. These need to be investigated in the future.

Acknowledgement

The financial support of this study by the engineering division of National Science Council of Taiwan, ROC through the contract NSC 89-2212-E009-074 is greatly appreciated.

References

[1] E.L. Koschmieder, S.G. Pallas, Heat transfer through a shallow horizontal convecting fluid layer, Int. J. Heat Mass Transfer 17 (1974) 991–1002.
[2] M. Akiyama, G.J. Hwang, K.C. Cheng, Experiments on the onset of longitudinal vortices in laminar forced convection between horizontal plates, ASME J. Heat Transfer 93 (1971) 335–341.
[3] Y. Kamotani, S. Ostrach, Effect of thermal instability on thermally developing channel flow, ASME J. Heat Transfer 98 (1976) 62–66.
[4] S. Ostrach, Y. Kamotani, Heat transfer augmentation in laminar fully developed channel flow by means of heating from below, ASME J. Heat Transfer 97 (1975) 220–225.
[5] M.Y. Chang, C.H. Yu, T.F. Lin, Changes of longitudinal vortex roll structure in a mixed convective air flow through a horizontal plane channel: an experimental study, Int. J. Heat Mass Transfer 40 (2) (1997) 347–363.
[6] K.C. Chiu, F. Rosenberger, Mixed convection between horizontal plates—I. Entrance effects, Int. J. Heat Mass Transfer 30 (1987) 1645–1654.
[7] K.C. Chiu, J. Ouazzani, F. Rosenberger, Mixed convection between horizontal plates—II. Fully developed flow, Int. J. Heat Mass Transfer 30 (1987) 1655–1662.
[8] H.K. Moffat, K.F. Jensen, Complex flow phenomena in MOCVD reactors, J. Crystal Growth 77 (1986) 108–119.
[9] H.K. Moffat, K.F. Jensen, Three-dimensional flow effects in silicon CVD in horizontal reactors, J. Electrochem. Soc. 135 (1988) 459–471.
[10] Y. Kamotani, S. Ostrach, H. Miao, Convective heat transfer augmentation in thermal entrance regions by means of thermal instability, ASME J. Heat Transfer 101 (1979) 222–226.
[11] J.W. Ou, K.C. Cheng, R.C. Lin, Natural convection effects on Graetz problem in horizontal rectangular channels with uniform wall temperature for large *Pr*, Int. J. Heat Mass Transfer 15 (1974) 835–843.
[12] F.C. Chou, G.J. Hwang, Vorticity-velocity method for the Graetz problem and the effect of natural convection in a horizontal rectangular channel with uniform wall heat flux, ASME J. Heat Transfer 109 (1987) 704–710.
[13] H.V. Mahaney, S. Ramadhyani, F.P. Incropera, Development of laminar mixed convection flow in a horizontal rectangular duct with uniform bottom heating, Numer. Heat Transfer 12 (1987) 137–155.
[14] C.C. Huang, T.F. Lin, Buoyancy induced flow transition in mixed convective flow of air through a bottom heated horizontal rectangular duct, Int. J. Heat Mass Transfer 37 (1994) 1235–1255.
[15] C.C. Huang, T.F. Lin, Vortex flow and thermal characteristics in mixed convection of air in a horizontal rectangular duct: effects of Reynolds and Grashof numbers, Int. J. Heat Mass Transfer 38 (1995) 1661–1674.
[16] D.G. Osbrone, F.P. Incropera, Laminar, mixed convection heat transfer for flow between horizontal parallel plates with asymmetric heating, Int. J. Heat Mass Transfer 28 (1985) 207–217.
[17] D.G. Osbrone, F.P. Incropera, Experimental study of mixed convection heat transfer for transitional and turbulent flow between horizontal, parallel plates, Int. J. Heat Mass Transfer 28 (1985) 1337–1344.
[18] F.P. Incropera, A.L. Knox, J.R. Maughan, Mixed-convection flow and heat transfer in the entry region of a horizontal rectangular ducts, ASME J. Heat Transfer 109 (1987) 434–439.
[19] K.C. Cheng, L. Shi, Visualization of convective instability phenomena in the entrance region of a horizontal rectangular channel heated from below and/or cooled from above, Exp. Heat Transfer 7 (1994) 235–248.
[20] R.K. Shah, A.L. London, in: Laminar Flow Forced Convection in Ducts, Academic Press, New York, 1987, pp. 196–198.
[21] S.J. Kline, F.A. McClintock, Describing uncertainties in single-sample experiments, Mech. Eng. 75 (1953) 3–12.
[22] M.L. Hitchman, K.F. Jensen, Chemical Vapor Deposition (Principles and Application), Academic Press, San Diego, 1993 (Chapter 2).